

Snapshots of Ce₇₀ Toroid Assembly from Solids and Solution

Ian Colliard, Jessica C. Brown, Dylan B. Fast, A. Kirstin Sockwell, Amy E. Hixon, and May Nyman*



Cite This: <https://doi.org/10.1021/jacs.1c04095>



Read Online

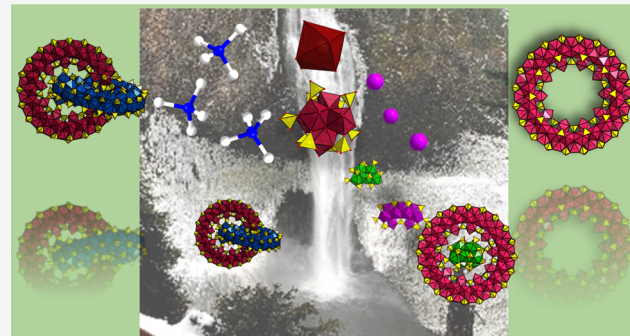
ACCESS |

Metrics & More

Article Recommendations

Supporting Information

ABSTRACT: Crystallization at the solid–liquid interface is difficult to spectroscopically observe and therefore challenging to understand and ultimately control at the molecular level. The Ce₇₀-toroid formulated [Ce^{IV}₇₀(OH)₃₆(O)₆₄(SO₄)₆₀(H₂O)₁₀]⁴⁻, part of a larger emerging family of M^{IV}₇₀-materials (M = Zr, U, Ce), presents such an opportunity. We elucidated assembly mechanisms by the X-ray scattering (small-angle scattering and total scattering) of solutions and solids as well as crystallizing and identifying fragments of Ce₇₀ by single-crystal X-ray diffraction. Fragments show evidence for templated growth (Ce₅, [Ce₅(O)₃(SO₄)₁₂]¹⁰⁻) and modular assembly from hexamer (Ce₆) building units (Ce₁₃, [Ce₁₃(O H)₆(O)₁₂(SO₄)₁₄(H₂O)₁₄]⁶⁻ and Ce₆₂, [Ce₆₂(OH)₃₀(O)₅₈(SO₄)₅₈]¹⁴⁻). Ce₆₂, an almost complete ring, precipitates instantaneously in the presence of ammonium cations as two torqued arcs that interlock by hydrogen bonding through NH₄⁺, a structural motif not observed before in inorganic systems. The room temperature rapid assemblies of both Ce₇₀ and Ce₆₂, respectively, by the addition of Li⁺ and NH₄⁺, along with ion-exchange and redox behavior, invite exploitation of this emerging material family in environmental and energy applications.



INTRODUCTION

A molecular building block approach is an important strategy to assemble bioinorganic, hybrid, and inorganic materials. It provides a level of control that is achievable in organic, hybrid organic–inorganic, and bioinorganic synthesis but is still emerging in purely inorganic synthesis. Rational bottoms-up design has been used to create DNA-nanostructures,^{1,2} peptide-nanostructures,^{3,4} inorganic macrocycles,^{5–9} metal–organic frameworks (MOFs),^{10,11} and metal–organic polyhedra.¹² Metal-oxo clusters (including polyoxometalates, POMs), which can be viewed as molecular metal-oxides, have greatly aided our ability to design purely inorganic materials with molecular-level precision. Such synthetic approaches are essential for optimizing materials function, including catalysis,¹³ magnetism,^{14–18} and luminescence.^{19,20} Building-block synthetic approaches have been hypothesized in metal-oxo systems including (1) assembly of Pd₈₄ and Pd₇₂ Pd-oxo toroids from a Pd₆ fragment,^{21–23} (2) Mn₈₄ and Mn₇₀ built from a Mn₁₂ oxo-acetate,^{24,25} (3) growth of giant molybdate POMs from smaller clusters,^{26,27} (4) assembly of successively larger Ln_x species (x = 12–140) from a Ln₄ oxocluster building unit,^{18,28–31} (5) isolation of various sized Ln_xNi_y-oxoclusters (up to 164 metal polyhedra) from smaller oxocluster building blocks,^{15,32,33} and (6) capping and linking of POMs into rigid chains and frameworks, and flexible polymers.^{34–36}

The d-block and f-block tetravalent metal cations (M^{IV}=Zr/Hf/Ce/U/Np/Pu^{IV}) are among the most studied metal-oxo cluster families. Of special note, Zr/Hf MOFs are built of the

M₆(OH,O)₈ hexamer (M₆), and these MOFs are widely exploited for virtually every application that has been developed to date including catalysis and separations.³⁷ The M₆ cluster is contained within most M^{IV}-oxoclusters as well as in fluorite-type MO₂; but it is not possible to simply build MO₂ (and intermediate size clusters such as M₃₈^{38–44}) from M₆-units, since the M₆-units share M₂ edges in the larger assemblies. In fact, M₆ is shown to coexist in solution with monomers, dimers and hexamers,^{45,46} likely in dynamic equilibrium. This demonstrates that models of metal-oxo cluster building block approaches such as M₆ → [intermediates] → MO₂ are oversimplified, and ultimately, scientists still lack control over the assembly processes in the M^{IV}-oxocluster families.

Ce-oxo clusters have been gaining importance and attention as molecular models of nano-CeO_x catalysts as well as functional catalysts themselves. The Ce^{III/IV} redox activity, without changes in coordination geometry, distinguishes this family of metal-oxo clusters: Ce₁₉, Ce₂₂, Ce₂₄, Ce₄₀ and Ce₁₀₀ oxoclusters have distinct Ce^{III} and Ce^{IV} sites,^{44,47,48} while Ce₃₈ reports mixed Ce^{III/IV} sites.⁴⁹ Given the rapidly growing

Received: April 19, 2021

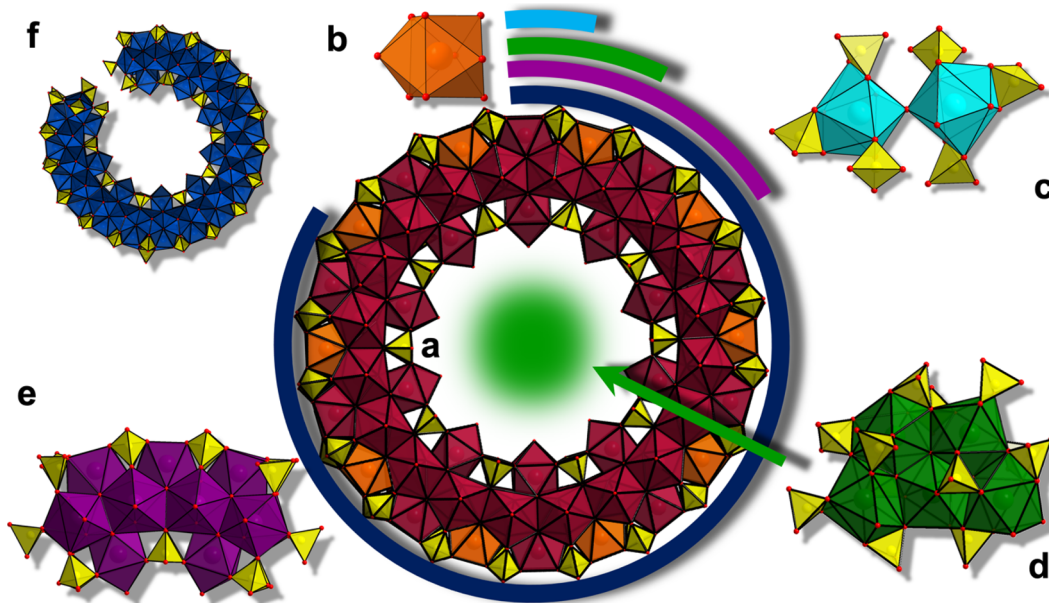


Figure 1. (a) Schematic showing isolated fragments of the Ce_{70} ring. (b) Monomer, $[\text{Ce}(\text{H}_2\text{O})_9]^{3+/4+}$, (c) oxo-bridged dimer $[\text{Ce}_2^{\text{IV}}-\text{O}(\text{SO}_4)_4]$, (d) $[\text{Ce}_5\text{O}_3(\text{SO}_4)_{12}]^{10-}$ pentamer that serves as a template, (e) $[\text{Ce}_{13}(\text{OH})_6(\text{O})_{12}(\text{SO}_4)_{14}]^{6-}$, (f) $[\text{Ce}_{62}(\text{OH})_{30}(\text{O})_{58}(\text{SO}_4)_{58}]^{14-}$.

interest in large molecular Ce-oxo clusters, we provide a summary of those of nuclearity >10 (plus brief synthesis information) in Table S21, including those reported here. The $\text{M}^{\text{IV}}_{70}$ sulfate ring structure, originally described for $\text{U}^{\text{IV}}_{70}$, followed by $\text{Ce}^{\text{IV}}_{70}$ and Zr_{70} ,^{50–53} is the only M^{IV} -topology besides M_6 that spans transition metals, lanthanides, and actinides and is also the largest. The hexamer units are distinct in M_{70} , alternating with monomers around the ring (Figure 1a). This unique arrangement presents an opportunity to study building-block assembly mechanisms. Ce_{70} and U_{70} have thus far been crystallized with mild hydrothermal heating. The transition metals and lanthanides that serve as counter-cations and also link the rings into intricate frameworks probably necessitate the heating to promote complete dissolution.^{50–52} In fact, Zr_{70} has been isolated at room temperature, as either a neutral form with no counter-cations or as a Na-salt,⁵² supporting this hypothesis. The neutral cluster also challenges our understanding of the role of the counter-cations.

We present here two strategies to capture incomplete fragments of the Ce_{70} -toroid that elucidate assembly pathways. The first strategy is to increase the heterometal (counter-cation) concentration in solution to inhibit full-ring formation. The second strategy is the use of ammonium counter-cations, which universally (for M^{IV}) promotes extremely rapid assembly of solution-phase species: in this case, nearly complete Ce_{62} -rings. Three Ce_{70} -fragments are observed by single crystal X-ray diffraction (SCXRD) including Ce_5 , Ce_{13} , and Ce_{62} (Figure 1). Pairs of torqued Ce_{62} open rings mutually stabilize each other by interlocking via H-bonding to ammonium, and X-ray scattering studies show that this fascinating interlocking suprastructure assembles immediately at room temperature. Ce^{III} added during the crystallization process replaces the ammonium, connecting the incomplete rings. The Ce_5 -fragment, based on its position just above and below the center of the complete Ce_{70} -ring, indicates templating ring growth from smaller fragments, similar to the templating of the Mo_{150} wheel from Mo_{36} .⁵⁴ Ce_{13} and Ce_{62} indicate the Ce_{70} -ring is formed by a building block approach, where building block

and templating mechanisms are by no means mutually exclusive.

Finally, we track room-temperature, *in situ* assembly via small-angle X-ray scattering (SAXS) of $\text{Ce}(\text{SO}_4)_2\text{-LiNO}_3$ solutions. SAXS indicates that the addition of Li^+ promotes Ce_{70} formation, but the assembly of rings and crystallization as a solid is likely nearly simultaneous. Ultimately, Ce_{70} crystallizes out of this *in situ* study, confirming the observed solution species. This differs from classic POM or aluminum polycation^{55–58} systems in which pH is clearly the driver of solution phase assembly while counterions promote crystallization: two distinct roles. In this system, the countercation is the driver of simultaneous assembly and crystallization, highlighting the importance of this often-overlooked parameter in prescribing aqueous inorganic reaction mechanisms.⁵⁹ In one final structure, we show that lanthanides (Yb^{3+}) can also serve as counterions and framework builders for the Ce_{70} -ring, and the entire family of Ce_{70} and Ce_{62} materials readily undergo cation exchange.

RESULTS AND DISCUSSION

All tetravalent metal cations form complexes with water molecules upon dissolution and exhibit strong hydrolysis tendencies. Oligomer formation due to hydrolysis and condensation reactions occurs even in acidic conditions,⁶⁰ and this is accelerated with heat or the addition of base. If uncontrolled, this process leads to metal oxide precipitation. The addition of heterometal cations and strongly coordinating oxoanion ligands can compete with the fundamental hydrolysis, solvation, and oxidation reactions that drive oligomerization. Most crystalline phases reported here were obtained from $\text{Ce}^{\text{IV}}(\text{SO}_4)_2$ solutions with added ammonium, Ni^{2+} or Yb^{3+} , heated at 75 °C. The exception is the Li^+ salt of Ce_{70} , obtained at room temperature. Details of syntheses are summarized in the SI.

Ce_{70} , $[\text{Ce}^{\text{IV}}_{70}(\text{OH})_{36}(\text{O})_{64}(\text{SO}_4)_{60}]^{4-}$, was described before and is also isostructural with Zr_{70} and U_{70} .^{50–53} Briefly, the Ce_{70} cluster can be viewed as ten Ce_6 -hexamers that alternate

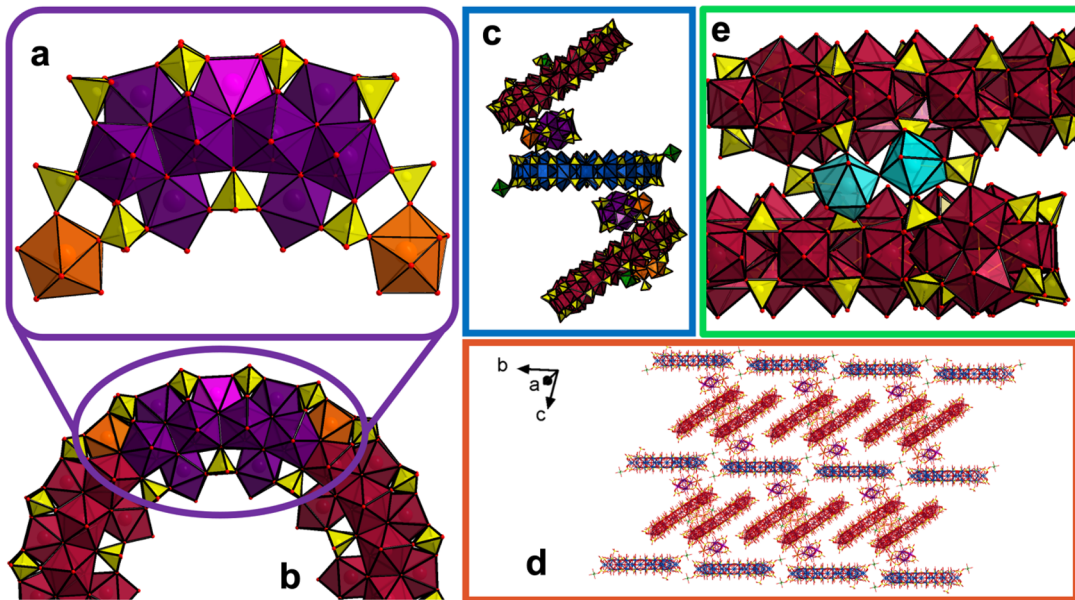


Figure 2. Polyhedral representation of (a) Ce_{13} fragment as crystallized in the $\text{NiCe}_{70}\text{-PacMan}$; Ce_{13} can be described as two Ce_6 in purple and the linking monomer in pink, the neighboring sulfate bridged Ce^{III} -monomers are shown in orange. (b) The relation of the Ce_{13} and surrounding monomers to the Ce_{70} ring, showing that Ce_{13} is a fragment in potential stepwise growth. (c) The entire building unit of the $\text{NiCe}_{70}\text{-PacMan}$ framework, Ni in green, sulfates in yellow, addenda sulfates omitted for clarity, sandwiched Ce_{70} in blue, and terminal Ce_{70} in red. (d) Wireframe representation of extended stacking of the $[(\text{Ce}_{13})_2\text{Ce}_{70}(\text{Ce}_{70})_2]$ -unit. (e) $[\text{Ce}_2^{\text{III}}\text{-O}]$ dimer in light blue bridging two Ce_{70} .

with ten Ce_1 -monomers. Four sulfates bridge each Ce_6 and Ce_1 along the outer rim, and four additional sulfates bridge only Ce_6 units along the inner rim. Each fragment discussed later can be viewed in the same context. The Ce_{62} , $[\text{Ce}_{62}(\text{OH})_{30}(\text{O})_{58}(\text{SO}_4)_{58}]^{14-}$, consisting of ~90% of the ring, contains nine Ce_6 and eight Ce_1 . Ce_{13} , $[\text{Ce}_{13}(\text{OH})_6(\text{O})_{12}(\text{SO}_4)_{14}(\text{H}_2\text{O})_{14}]^{6-}$, consists of two Ce_6 and Ce_1 and is approximately 20% of the ring. Ce_5 , $[\text{Ce}_5(\text{O})_3(\text{SO}_4)_{12}]^{10-}$ resembles half of the Ce_6 plus two flanking monomers. These clusters and their intrinsic relation to the Ce_{70} , summarized in Figure 1, serve as crystallographic snapshots of mechanistic pathways for ring formation.

NiCe₇₀-PacMan and the Ce₁₃ Fragment. Previously, we obtained a Ni-linked Ce_{70} framework from a solution of ~2:1 Ce:Ni. In the previous study of TM-linked Ce_{70} (TM = transition metal) frameworks, we observed a general trend where an increase in the TM concentration in reaction solutions yielded frameworks with a greater incorporation of Ce-monomers, *instead* of the TM-linkers.⁵² This result was initially counterintuitive but attributable to the TMs inhibiting or slowing Ce_{70} formation. The Ce-monomers are important in these frameworks because they are either mixed $\text{Ce}^{\text{IV}/\text{V}}$ or purely Ce^{III} oxidation state, where both oxidation states were shown to be redox active in the monomer form. Here, increasing the Ni:Ce ratio to almost 1:1, we obtained the $\text{NiCe}_{70}\text{-PacMan}$ phase (triclinic space group $P-1$, $V = 63,794(9)$ Å³, Table S1) that features the Ce_{13} -fragment (Figure 2, see SI for synthesis details). $\text{NiCe}_{70}\text{-PacMan}$, named for the resemblance of the $\text{Ce}_{70}\text{-Ce}_{13}\text{-Ce}_{70}$ unit to the 1980s video game character (Figure 2c), is described by the moiety formula $[\text{Ni}(\text{H}_2\text{O})_6]_2 \mu - [(\text{Ni}(\text{H}_2\text{O})_5)(\text{Ce}^{\text{IV}}_2(\text{H}_2\text{O})_{5.5})_2(\text{Ce}_{13}(\text{OH})_6(\text{O})_{12}(\text{SO}_4)_{14}(\text{H}_2\text{O})_{14})_2\text{Ce}_{70}(\text{OH})_{36}(\text{O})_{64}(\text{SO}_4)_{60}(\text{H}_2\text{O})_{45}] \mu - [\text{Ce}_2^{\text{III}}\text{-O}(\text{SO}_4)_4(\text{H}_2\text{O})_8] - [\text{Ni} - \text{Ce}^{\text{III}}_{1.5}\text{Ce}_{70}(\text{OH})_{36}(\text{O})_{64}(\text{SO}_4)_{61.75}(\text{H}_2\text{O})_{44}]_2$. The framework is shown in Figure 2d. Along the b -direction, there are

approximate layers of Ce_{70} rings (blue). The layers alternate with stacks of offset Ce_{70} , tilted from the former layers by ~30° (red). The latter Ce_{70} -rings are dimerized, linked by an unusual linear $\text{Ce}^{\text{IV}}_2\text{-O}$ dimer unit (Figure 2e). The linear unit ($\text{Ce}-\text{O}-\text{Ce}$ angle = 179.99(6)°) resembles a recently described $\text{Pu}-\text{O}-\text{Pu}$ dimer isolated as a nitrate salt, highlighting a similarity between these f-block elements.⁶¹ Of the $[\text{Ce}_{70}]_2$ -dimer, one forms the Ce_{13} -“pacman” unit with Ce_{70} of the layer above and the second with the layer below. All Ce_{70} rings present the same core formula as above.

The Ce_{13} fragment is of particular note because it provides a snapshot of the stepwise assembly pathway for the formation of the Ce_{70} ring, as illustrated in Figure 2a,b. The fragment consists of two hexamers with a bridging monomer in the exact arrangement as that observed in Ce_{70} . Bond valence analysis (BVA) of Ce and O for the fragment confirms the overall formula of $[\text{Ce}_{13}(\text{OH})_6(\text{O})_{12}(\text{SO}_4)_{14}(\text{H}_2\text{O})_{14}]^{6-}$ with all Ce^{IV} (Tables S11, S12). The fragment is capped on either side by Ce-monomers which are Ce^{III} (Figure 2a, Table S15). While the Ni^{II} concentration of the reaction solution appears to play a role in isolation of the Ce_{13} -fragment, it is very sparse in the isolated framework. All three crystallographically unique Ni^{II} sites are regular $\text{Ni}(\text{H}_2\text{O})_5(\text{O}-\text{SO}_3)$ or $\text{Ni}(\text{H}_2\text{O})_6$ octahedra decorating the Ce_{70} rings (green polyhedra/spheres in Figures 2c,d) with bond lengths from 1.98 to 2.03 (2) Å (BVS = 2.1–2.2; see Tables S9, S13). The abundant Ni^{II} in the reaction solution is the most likely reagent for the Ce^{IV} to Ce^{III} reduction, even though all nickel present in the structure is divalent.

Ammonium Counterions for Fragment Isolation. Ammonium counterions are complex and unpredictable. They are both a weak acid and a weak base. They have a larger effective radius than TM or Ln cations and are unable to directly bind directly to sulfate.⁶² However, they can undergo strong H-bonding in solution and in solids. In our experience, ammonium salts of metal oxo clusters (i.e., polyoxometalates)

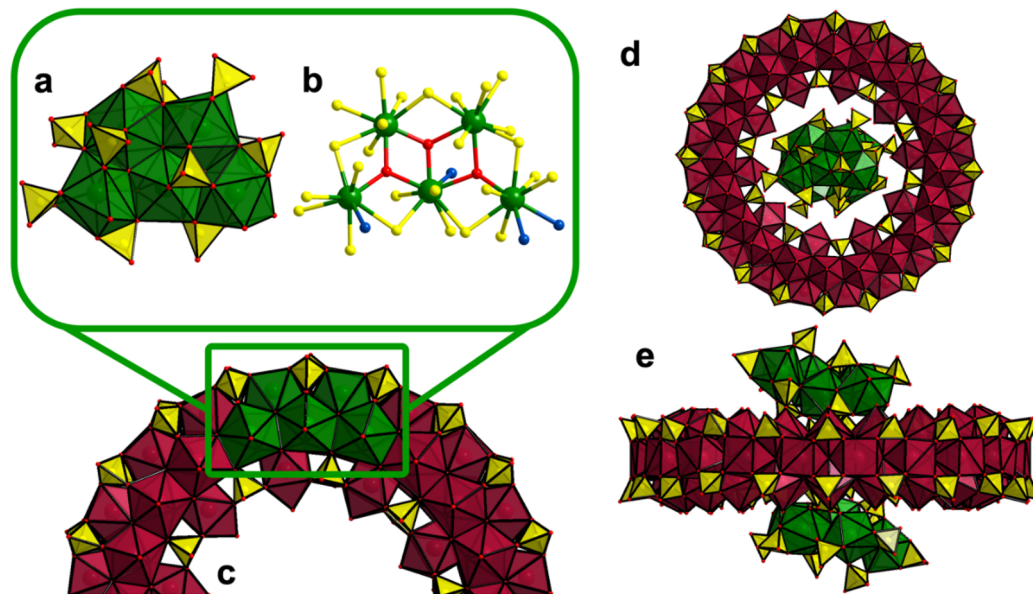


Figure 3. (a) Polyhedral representation of Ce₅ and (b) ball and stick representation of Ce₅ cluster with the Ce in green, μ₃-oxos in red, oxygens from sulfates in yellow, and aqua oxygens in blue. (c) Polyhedral representation of Ce₅ in relation to the Ce₇₀, (d) top view showing the location of the Ce₅ in the inner void of the Ce₇₀, and (e) side showing the location of the Ce₅ in the inner void sandwiching a Ce₇₀, ammoniums omitted for clarity.

can be either very soluble or very insoluble, depending on the charge of the cluster. The synthesis of Ce^{IV}-SO₄²⁻-NH₄⁺ compounds reported here differs from the analogous TM or lanthanide Ce^{IV}-SO₄ reactions. Namely, with TM (i.e., NiCe₇₀-PacMan) or lanthanides (discussed below), the reaction solutions go into the oven completely dissolved, and the Ce₇₀-frameworks crystallize during the 75 °C hydrothermal treatment. The analogous ammonium reaction solutions precipitate immediately upon preparation at room temperature (amorphous precipitate, discussed below), then redissolve upon heating, and come out of the 75 °C oven completely dissolved. The lattices crystallize only upon cooling to room temperature, over the course of a day. The ammonium reactions have yielded several crystal structures, precipitates, and solutions that provide further insight into assembly pathways.

NH₄(Ce₅)₂Ce₇₀, fully formulated as (NH₄)₅₂[Ce₅(O)₃(SO₄)₁₂(H₂O)₄]₂Ce₇₀(OH)₃₆-(O)₆₄(SO₄)₇₄(H₂O)₃₆, crystallizes in the monoclinic space group I2/a (V = 74,657 (1) Å³, Table S2). With no linking TM or Ce^{III/IV} monomers, the Ce₇₀ rings are not connected into extended frameworks. However, the Ce₇₀ rings are sandwiched between two Ce₅ fragments, which sit just above and below the center of the wheel in a manner that implies templating.

The Ce₅ cluster is formulated as [Ce₅(O)₃(SO₄)₁₂(H₂O)₄]¹⁰⁻. The five Ce-centers are assembled in a nearly planar trapezoidal shape with three bridging oxos between the three centers, shown in red in Figure 3a,b. Each Ce is 8–9 coordinate, and the remainder of the coordination sphere is completed with bridging and chelating sulfates; no hydroxides are recognized in this unit. BVA of the pentamer confirms a tetravalent charge for these Ce (Table S16). The pentameric units cap the inner diameter of the rings, bridged by ammonium hydrogen bonding, with distances ~2.7–3.2 Å. Although we can recognize exactly this pentamer fragment in the Ce₇₀-ring (Figure 3c), especially the

arrangement of the oxo-units, we are biased to think that the hexamer and monomer units are the modular building units for Ce₇₀ (as well as the U^{IV} and Zr^{IV} analogues). This bias stems from the numerous structures featuring the [M^{IV}₆O₄(OH)₄] core for M = Zr, Hf, Ce, Th, U, Np, and Pu.

Isolation of the Ce₅-cluster fragment provides some insight into assembly pathways of Ce₇₀, namely, multiple related and similar-sized cluster geometries can form simultaneously; i.e., Ce₅ and Ce₆ (not necessarily just the ones that crystallize). Ce₅ contains only oxo bridges, no hydroxyl bridges. Most isolated Ce₆-hexamer clusters^{63,64} as well as within Ce₇₀ alternate oxo and hydroxyl bridges. Oxo vs hydroxyl bridges in aqueous acidic reaction solutions such as these are controlled by solution pH, acidity of M^{IV}, and geometry of assemblies. It is difficult to determine by any spectroscopic means if Ce₅ forms earlier, later, or simultaneously with Ce₆ in the reaction process. If our initial hypothesis is correct and Ce₆ is the main building block of Ce₇₀ assembly, then Ce₅ forms as a minor component along with Ce₆ (since it is not isolated as a pure phase), and it is a “reject” of the dominant Ce₇₀ assembly pathway. The juxtaposition of Ce₅ to Ce₇₀ in the crystalline lattice (Figure 3d,e) could imply templating of Ce₇₀ by smaller units or alternatively, adventitious siting of Ce₅ on the Ce₇₀ face during crystal formation (see schematic Figure S2c).

Crystallization of the various ammonium-supported structures is dictated by NH₄⁺-concentration. Crystal formation of NH₄(Ce₆₂)₂ (described below) occurred at a Ce:NH₄⁺ molar ratio range of ~1:20–1:30. No crystal growth is observed at ratios lower than 1:20, and the ammonium cerium sulfate monomer salt was crystallized at ratios higher than 1:30. The NH₄(Ce₆₂)₂ is the only structure that can be obtained as a relatively pure phase at ~1:25 ratio, with NH₄(Ce₅)₂Ce₇₀ (described above) cocrystallizing at a ~1:20 ratio and the NH₄Ce₇₀ cocrystallizing at ~1:30. This indicates the interlocked Ce₆₂ rings are quite stable and stabilized by ammonium since they are not observed with any other counterion. Varying reaction conditions and reagents to

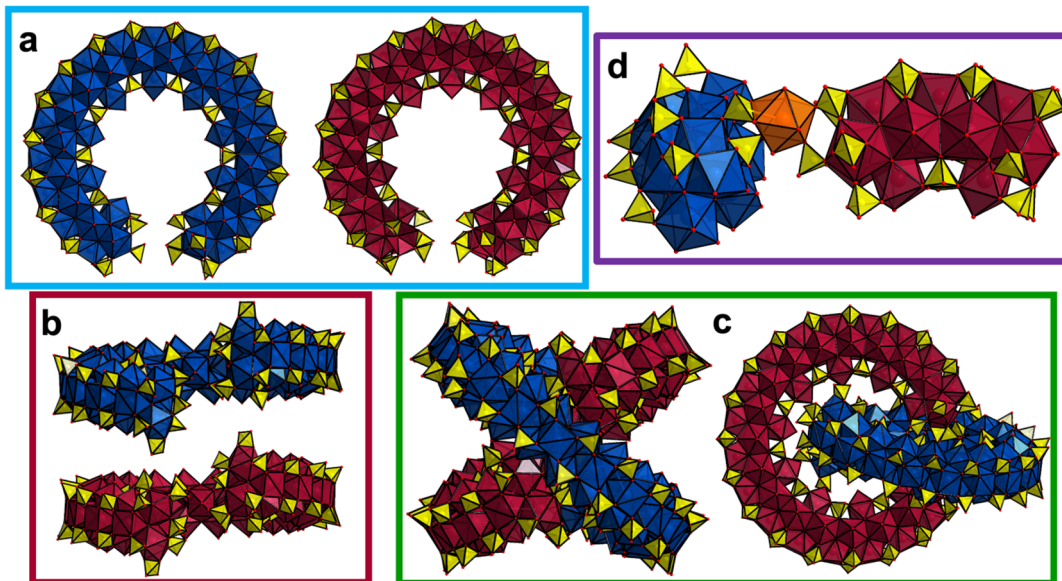


Figure 4. Polyhedral representation of (a) top view of the two crystallographically unique Ce_{62} shown in blue and maroon, (b) side view of the two unique Ce_{62} showing the ends misaligned, (c) side view and top view of the $[\text{Ce}_{62}]_2$ -dimer d) incorporation of the Ce^{III} -monomer in orange at the end of a Ce_{62} in red coordinating partway the blue Ce_{62} , sulfate in yellow, addenda sulfate and ammoniums omitted for clarity and oxygens in red.

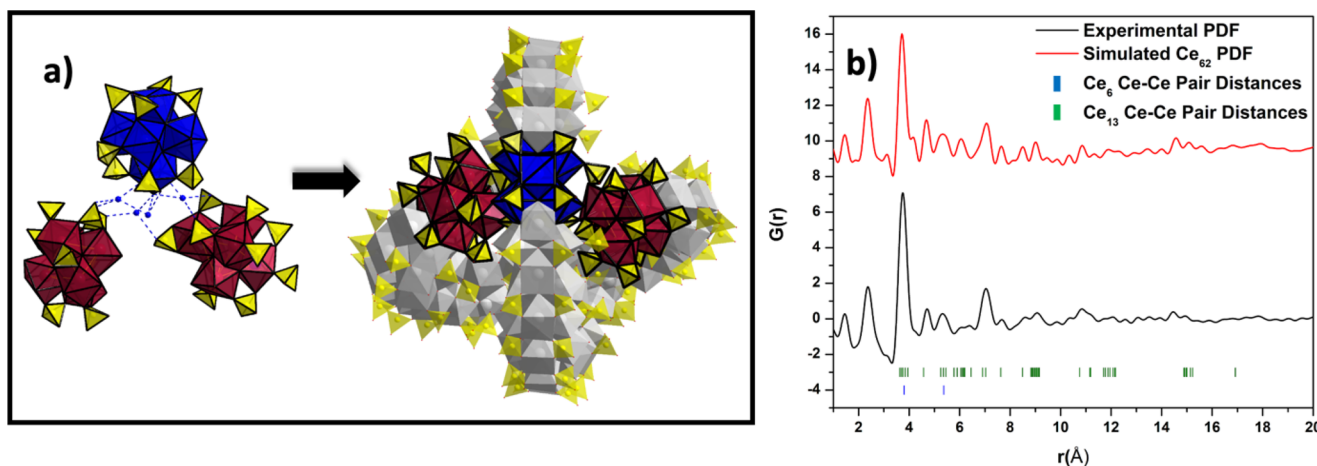


Figure 5. (a) Proposed mechanism of $[\text{Ce}_{62}]_2$ dimer assembly, templated by ammonium. On the left, three hexamers associate by H-bonding through associated NH_4^+ -cations (blue spheres, blue dotted lines show H-bonding, $\text{H}_4\text{N}-\text{O}_{\text{sulfate}}$ or $\text{H}_4\text{N} \cdots \text{O}_{\text{Ce}}$ distances are in the range of 2.7–3.0 Å). The blue Ce_6 is at the center position (5th hexamer from either open-end) of one Ce_{62} , and the maroon hexamers are the end-caps to the other Ce_{62} . The image on the right indicates the same Ce_6 -hexamers highlighted in the $[\text{Ce}_{62}]_2$ dimer. (b) Simulated PDF for $\text{NH}_4(\text{Ce}_{62})_2$ compared to experimental scattering for amorphous $\text{Ce}(\text{SO}_4)_2$ plus NH_4^+ precipitate. Tick marks at the bottom indicate expected Ce–Ce pair distances in the Ce_6 and Ce_{13} clusters.

isolate pure phases for $\text{NH}_4(\text{Ce}_5)_2\text{Ce}_{70}$ and $\text{NH}_4\text{Ce}_{70}$ were not successful: $\text{NH}_4(\text{Ce}_{62})_2$ was always the most prominent phase.

$\text{NH}_4(\text{Ce}_{62})_2$, formulated as $(\text{NH}_4)_82(\text{Ce}_{62}(\text{OH})_{30}(\text{O})_{58}(\text{SO}_4)_{71}(\text{H}_2\text{O})_{33.25})$ ($\text{Ce}_{62}(\text{OH})_{30}(\text{O})_{58}(\text{SO}_4)_{72}(\text{H}_2\text{O})_{29.75}$), crystallizes in the triclinic space group $P-1$ ($V = 58,252$ (4) Å³, Table S3). The Ce_{62} cluster, formulated $[\text{Ce}_{62}(\text{OH})_{30}(\text{O})_{58}(\text{SO}_4)_{58}]^{14-}$, is missing a single hexamer and two monomers to complete a full Ce_{70} (Figure 4a). Addenda sulfates decorate the partially formed rings and serve as interaction points to the neighboring fragments via H-bonding ammoniums. The ring fragments dimerize almost perpendicular to each other, with a 14° torsion between both ends of the fragments (Figure 4b,c). Ce–O bond distances within Ce_{62} (Table S17) are comparable with those of Ce_{70} (Table S9), suggesting the strain of the torsion is

delocalized throughout the open ring. The sulfates capping the ring-ends are partially occupied, consistent with lability, allowing completion of the ring under appropriate conditions. The completed Ce_{70} ring with no other building units is obtained as minor cocrystallites along with Ce_{62} crystals, in two different unit cells. See Figures S5, S6 and Tables S5, S6 for additional information.

Pair distribution function (PDF) analysis of the amorphous solid that precipitates upon the preparation of $\text{NH}_4(\text{Ce}_{62})_2$ reaction solutions ($(\text{NH}_4)_2\text{SO}_4$ plus $\text{Ce}(\text{SO}_4)_2$) provides compelling evidence that the Ce_{62} -ring begins to form immediately upon combining $\text{Ce}(\text{SO}_4)_2$ and NH_4^+ (Figures 5b and S13). Pair correlations out to ~14.5 Å are observed and are largely attributable to Ce–Ce distances, due to their high scattering strength in comparison to other elements present in

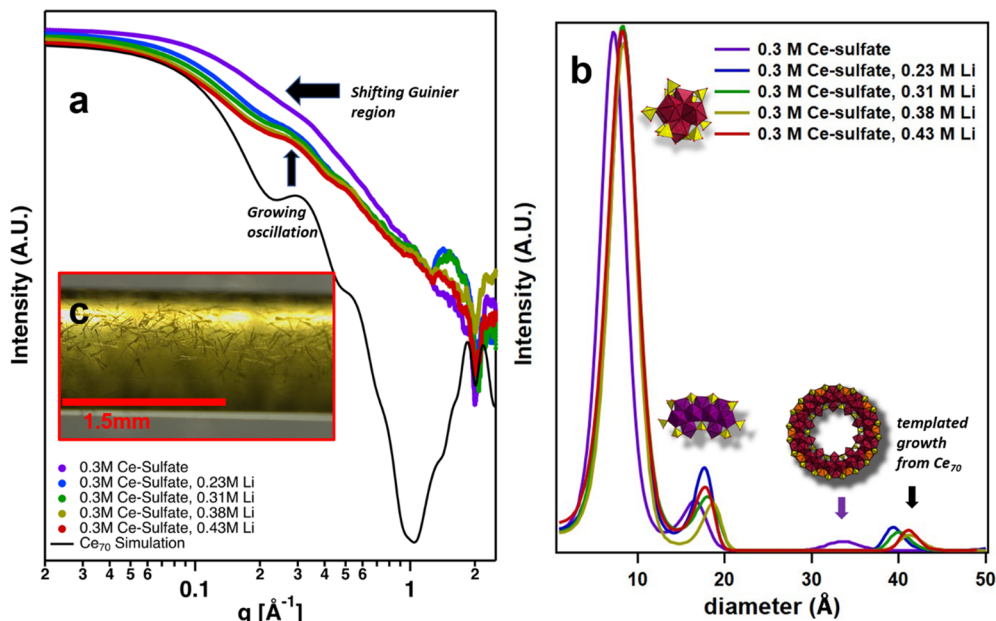


Figure 6. (A) Small angle X-ray scattering curves of $\text{Ce}(\text{SO}_4)_2$ with increasing addition of lithium nitrate. (B) Size distribution analyses of the scattering curves that show predominantly Ce_6 hexamers ($\sim 90\%$), species similar in size to Ce_{13} (6–10%), and templated growth off of Ce_{70} (1–3%). (C) Microscope image of LiCe_{70} crystals growing inside the SAXS capillary.

the material. While this precipitate may be a mixture of the species proposed in this paper, only larger species, such as the Ce_{62} or Ce_{70} rings or even Ce_{13} , have Ce–Ce pairs at 14.5 \AA . The experimental and simulated PDF match well, with the most notable exception being a weaker than expected minor peak just above 6 \AA that corresponds to Ce–Ce pairs on the inner edge of the ring fragments. This discrepancy may be attributable to a degree of flexibility of this open ring structure at room temperature that broadens the signal at this pair distance. This suggests further manipulations of the open ring may be possible, if we are able to dissolve this material in appropriate conditions. Finally, the scattering spectrum from 5 to 50° , 2θ (Mo–K α ; figure S13), presents similar features as the spectrum simulated from the single-crystal structure of $\text{NH}_4(\text{Ce}_{62})_2$. However, diffraction peaks are broader with fewer features in the experimental spectrum than those for the calculated spectrum, as expected for a disordered structure.

Along with consideration of assembly mechanisms and the role of the ammonium, room temperature SAXS of $\text{Ce}(\text{SO}_4)_2$ alone suggests it consists of 90% hexamer-sized species, and 10% larger species (Figure 6a, purple curve), discussed later. This means these small cluster building blocks (Ce_6) assemble immediately from the monomer salt, likely due to Ce^{IV} acidity creating O/OH linkages as well as the tendency of sulfate ligands to bridge and cap.

Addition of the ammonium as either a sulfate, nitrate salt, or acetate salt also produced rapid precipitation, affirming the NH_4^+ is responsible for the rapid assembly of Ce_{62} interlocking rings. Inspection of the $\text{NH}_4(\text{Ce}_{62})_2$ structure along with the $\text{Ce}(\text{SO}_4)_2$ SAXS data (dominated by hexamers) provides compelling evidence that the $(\text{Ce}_{62})_2$ assembly is initiated at the point of linkage between the two rings. Figure 5a highlights this region of the structure, showing the two end-hexamers of one Ce_{62} (maroon) connecting the fifth (central) hexamer in the middle of the adjoining Ce_{62} (blue). Between these three hexamers is a strong H-bonded network of ammonium cations; $\text{H}_4\text{N}-\text{O}_{\text{sulfate}}$ or $\text{H}_4\text{N}-\text{O}_{\text{Ce}}$ distances are in the range of 2.7 – 3.0

\AA . There is a similar network between the two end hexamers and the hexamers that flank the central hexamer (4th and sixth) of the adjoining Ce_{62} . In summary, the highlighted area in Figure 5a is likely the nucleation point of assembly of the interlocking $(\text{Ce}_{62})_2$, from the prevalent hexamers. Thus, we hypothesize that Ce_{62} grows symmetrically from either the end hexamers (maroon) or the central hexamer (blue). It is possible that the second connection point of the interlocked $(\text{Ce}_{62})_2$ grows simultaneously. Nonetheless, the assembly mechanism, based on the combined solid-state and solution data, is hexamer-by-hexamer addition but with more complex growth paths than sequential addition around the ring.

Due to the unique synthesis of the ammonium-cerium assemblies, opportunity for synthetic modification emerges after hydrothermal processing but before crystallization of $\text{NH}_4(\text{Ce}_{62})_2$. As previously mentioned, the $\text{NH}_4^+ - \text{Ce}^{\text{IV}} - \text{SO}_4^{2-}$ solutions crystallize only upon being cooled from 75° C to room temperature. At this point, we can add heteroatoms to promote framework formation, and we demonstrated this with addition of CeCl_3 (see SI). When the solution was cooled, a new structure crystallized out. The $\text{NH}_4\text{Ce}(\text{Ce}_{62})_2$, formulated as $(\text{NH}_4)_7(\text{Ce}_{1.25}(\text{H}_2\text{O})_{4.5})(\text{Ce}_{62}(\text{OH})_{30}(\text{O})_{58}(\text{SO}_4)_{70}(\text{H}_2\text{O})_{31.5})(\text{Ce}_{62}(\text{OH})_{30}(\text{O})_{58}(\text{SO}_4)_{70}(\text{H}_2\text{O})_{33.25})$, crystallizes in the triclinic space group $P-1$ ($V = 59,403 (8) \text{ \AA}^3$, Table S4). The Ce^{III} -monomers are located at two of the four anchor points; one is fully occupied, and the second exhibits 1/4 occupancy (Figure 4d). BVA of the monomers confirms these are trivalent (Table S18).

Tracking Ce_{70} Formation in Solution. We used SAXS solution studies to track the formation of Ce_{70} in solution conditions where solubility is maintained, in particular, to determine the role of the counterion. Single crystal data often shows only the end result of solution processes; however, SAXS can provide insight into subtle changes in solution. Starting with the same $\text{Ce}(\text{SO}_4)_2$ solution concentration used for synthesis (0.3 M), cluster growth was promoted by the

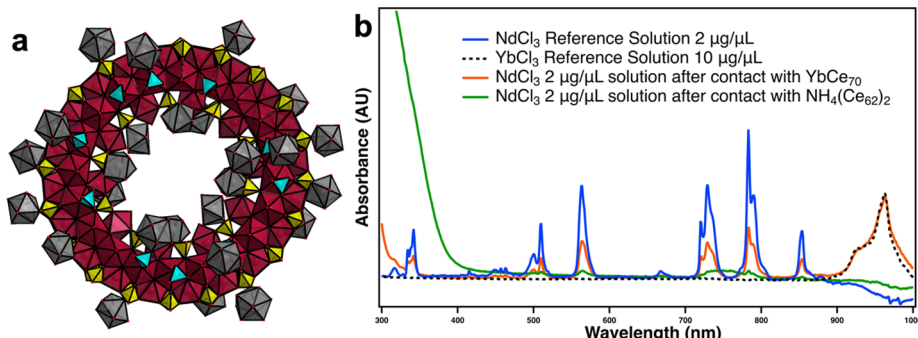


Figure 7. (A) Polyhedral Representation of YbCe₇₀ showing the Yb monomers in gray, Ce of Ce₇₀ in maroon, Ce₇₀ sulfates in yellow, addenda sulfates in turquoise, and oxygens red. (B) UV-vis spectra of Nd³⁺ solutions before and after contact with YbCe₇₀ and NH₄(Ce₆₂)₂. A Yb³⁺ reference solution confirms ion exchange between Nd and Yb for YbCe₇₀.

addition of LiOH (figure S10), wherein Li⁺ can serve as a counterion and the OH⁻ can drive hydrolysis. Li⁺ was chosen as the countercation to support solubility and to minimize competitive X-ray scattering. Even at high acidity and high concentration, dissolved Ce(SO₄)₂ shows a high degree of polymerization (discussed below). Increase of the pH from 0.75 (self-buffering) to 1.12, 1.38, and finally 1.70 with LiOH promoted assembly of larger species in solution, indicated by the shifting Guinier region to lower-q. In addition, distinctive features indicative of the Ce₇₀ shape and size are seen by the pair of peaks at high q (1.9 Å⁻¹ and 2.1 Å⁻¹) and by the growth of the oscillation around q = 0.3 Å⁻¹.^{50–53}

To differentiate the effects of increasing pH with increasing counterions, the experiment was repeated using LiNO₃ instead of LiOH and was found to be virtually identical. The LiNO₃-Ce(SO₄)₂ series is shown in Figure 6a. Both LiOH and LiNO₃ solutions crystallize Li-Ce₇₀ directly in the SAXS capillary (Figure 6c; structure reported below). Consistent with instantaneous [Ce₆₂]₂ formation and precipitation, this indicates that (1) Ce₇₀ is readily formed without forced hydrolysis by the addition of base or heating and (2) the main function of the counterion, whether it is ammonium, Ce-monomers, transition metals,⁵² or lanthanides (below), is to assemble, connect, and balance the very small charge (-4) of the ring. In fact, all structures produced to date have multiple addenda sulfates to charge balance the multiple polyvalent cations that are framework formers.

Size distribution analyses (Figure 6b) were performed on the SAXS curves to estimate species size and track their evolution with increasing Li⁺. The data is summarized in Table S19, and scattering curve fits are shown in Figure S11. The size distribution analysis of the simple Ce(SO₄)₂ solution suggests that 90% of the dissolved species is the Ce₆-hexamer, ~8% of the species is the approximate size of Ce₁₃, and ~2% were the size of the fully formed Ce₇₀ cluster. We do not expect to see a high concentration of Ce₇₀ due to its low charge/size ratio and, based on our past experience, we know Ce₇₀ is poorly soluble in water. There are likely Ce-monomers present as well, but scattering intensity scales as volume³ of the scattering species; thus, the minor fraction of larger species dominate the spectra. The intermediate size species (~15–18 Å in diameter) could also be a hexamer flanked by two monomers, Ce₁₃ flanked by two monomers, etc. As Li⁺ is added, the populations of these three identified species-sizes do not change significantly. However, each population gets larger in diameter (Figure 6b). The increase in the size of the Ce₆ and Ce₁₃-sized populations is most certainly an addition of monomers and

hexamers, as a stepwise ring growth. The increase in size is substantial for the Ce₇₀ population, ~ 25%. This could represent a minor amount of offset ring-stacking (Figure S12) seen in many M₇₀ crystal structures,^{50–53} as a prenucleation process,⁵¹ or ring fragments (Ce₆, Ce₁₃, etc.) assembling neighboring rings from the Ce₇₀ "scaffold". The small population of Ce₇₀ in solution represents equilibrium solubility and suggests formation and crystallization are essentially simultaneous. This is contrary to most POM systems where there is a distinct complete assembly, followed by crystallization.

Single crystal analysis confirmed the formation of LiCe₇₀ in these experiments. LiCe₇₀ is fully formulated as Li₂₈Ce₇₀(OH)₂₆(O)₆₄(SO₄)₇₇(H₂O)₃₅ and crystallizes in the orthorhombic space group *Pnma* ($V = 66,045$ (11) Å³, Table S7). In summary, SAXS provides conclusive evidence that the counterions are essential for ring-assembly and assembly of rings into crystalline lattices.

Ion Sorption and Exchange. We previously demonstrated that Ln^{III} are preferentially absorbed into TM^{II}Ce₇₀ frameworks due to the availability of coordinating sulfates, without evidence for ion exchange except for perhaps H₃O⁺.⁵² However, the role of Ln-counterions in the Ce₇₀-framework assembly was not known neither was the subsequent ion exchange behavior of the putative Ln-Ce₇₀ frameworks. At the same time, documentation of ion exchange behavior of NH₄(Ce₆₂)₂ provides further information about this unique phase.

Adoption of the TM^{II}Ce₇₀ synthesis to include Yb₂O₃ starting material instead of TM-salts (see SI, synthesis) yielded YbCe₇₀. This departs from the chemistry of the U^{IV} counterparts. U^{IV} favored U₇₀ with transition metals and the U₈₄ "superatom" with lanthanides.⁵⁰ However, given the demonstrated ease of assembly of Ce₇₀ in the SAXS study and Ce₆₂ with NH₄⁺ counterions, it is not surprising that the reaction product is not crucially dependent on the identity of the countercation/framework builders (with the exception of ammonium). YbCe₇₀ is fully formulated Yb₁₃Ce₇₀(OH)₃₆(O)₆₄(SO₄)_{77.5}(H₂O)_{106.5}; structural description and additional figures are included in the SI. Lanthanides, with their distinctive UV-vis spectra, provide a facile method to monitor ion-exchange: both Ln³⁺ that leaves the solution and enters the framework and vice versa. This is clearly demonstrated for the exchange of Yb³⁺ for Nd³⁺ in the YbCe₇₀ framework (Figure 7b). The Nd³⁺ peaks are diminished after contact with YbCe₇₀, and new peaks appear at 963 and 927 nm, consistent with free Yb³⁺ in solution. A titration

experiment (figure S13) indicates two Yb^{3+} ions per Ce_{70} exchange. Similarly, $\text{NH}_4^+(\text{Ce}_{62})_2$ exchanges in three Nd^{3+} per Ce_{62} (figure S13) or six per $\text{NH}_4^+(\text{Ce}_{62})_2$.

CONCLUSION

Multiple crystal structures featuring fragments of the Ce_{70} -ring, including a pentamer in a position that indicates templating, provide compelling evidence for a stepwise assembly of the rings. The X-ray scattering of amorphous precipitates along with solution phase scattering suggests a more complex mechanism ensues during insipient crystallization, where ring assembly and ordering into a solid-state lattice occur simultaneously. While transition metal, alkali, and lanthanide cations join the anionic Ce_{70} -rings into frameworks via bridging sulfates, their role in assembly is otherwise minimal, and perhaps the rings could be isolated without counterions, as was demonstrated with Zr_{70} .^{S2} The exceptional counterion is ammonium; in its presence, an interlocking dimer of Ce_{62} ring fragments assembles and precipitates spontaneously at room temperature. This twisted open ring is a motif that was previously unrecognized in inorganic metal-oxo cluster chemistry. We proposed a mechanism of nucleation and growth from the two open ends of the ring toward the middle, based on mutual templating and strong NH_4^+ H-bonding within the dimer. Facile rare earth ion exchange was demonstrated with both Ce_{70} and Ce_{62} phases. We believe the amorphous $\text{NH}_4^+-\text{Ce}_{62}$, very easily synthesized, will provide even better ion exchange properties (kinetics and capacity) that could also engage $\text{Ce}^{\text{III/IV}}$ redox and acid-catalysis activity. Catalysis studies are underway, in addition to the exchange of rare earth metals, actinides, and specific radionuclides of concern (i.e., ^{137}Cs , ^{90}Sr).

ASSOCIATED CONTENT

Supporting Information

The Supporting Information is available free of charge at <https://pubs.acs.org/doi/10.1021/jacs.1c04095>.

Details concerning synthesis, instrumentation, crystallography, crystallographic tables, summary of bond lengths and bond valence sum calculations, microscope images of crystals, ion-sorption studies, miscellaneous supplementary images, and table summarizing large cerium-oxo clusters synthesized to date ([PDF](#))

Accession Codes

CCDC 2057078, 2057085–2057086, 2057088–2057091, and 2064990 contain the supplementary crystallographic data for this paper. These data can be obtained free of charge via www.ccdc.cam.ac.uk/data_request/cif, or by emailing data_request@ccdc.cam.ac.uk, or by contacting The Cambridge Crystallographic Data Centre, 12 Union Road, Cambridge CB2 1EZ, UK; fax: +44 1223 336033.

AUTHOR INFORMATION

Corresponding Author

May Nyman – Department of Chemistry, Oregon State University, Corvallis, Oregon 97331, United States;
orcid.org/0000-0002-1787-0518; Email: may.nyman@oregonstate.edu

Authors

Ian Colliard – Department of Chemistry, Oregon State University, Corvallis, Oregon 97331, United States

Jessica C. Brown – Department of Chemistry, Oregon State University, Corvallis, Oregon 97331, United States
Dylan B. Fast – Department of Chemistry, Oregon State University, Corvallis, Oregon 97331, United States;
orcid.org/0000-0002-0888-4950

A. Kirstin Sockwell – Department of Civil and Environmental Engineering and Earth Sciences, University of Notre Dame, Notre Dame, Indiana 46556, United States; orcid.org/0000-0002-0382-2144

Amy E. Hixon – Department of Civil and Environmental Engineering and Earth Sciences, University of Notre Dame, Notre Dame, Indiana 46556, United States; orcid.org/0000-0003-4513-4574

Complete contact information is available at:
<https://pubs.acs.org/10.1021/jacs.1c04095>

Notes

The authors declare no competing financial interest.

ACKNOWLEDGMENTS

This work was supported by the Department of Energy, National Nuclear Security Administration (NNSA) under Award Number DE-NA0003763. We acknowledge the Murdock Charitable Trust (Grant No. SR-2017297) for acquisition of the single-crystal X-ray diffractometer.

REFERENCES

- Douglas, S. M.; Dietz, H.; Liedl, T.; Höglberg, B.; Graf, F.; Shih, W. M. Self-assembly of DNA into nanoscale three-dimensional shapes. *Nature* **2009**, *459* (7245), 414–418.
- Perez-Romero, A.; Dominguez-Martin, A.; Galli, S.; Santamaría-Díaz, N.; Palacios, O.; Dobado, J. A.; Nyman, M.; Galindo, M. A. Single-Stranded DNA as Supramolecular Template for One-Dimensional Palladium(II) Arrays. *Angew. Chem., Int. Ed.* **2021**, *60* (18), 10089–10094.
- Whaley, S. R.; English, D. S.; Hu, E. L.; Barbara, P. F.; Belcher, A. M. Selection of peptides with semiconductor binding specificity for directed nanocrystal assembly. *Nature* **2000**, *405* (6787), 665–668.
- Gazit, E. Self-assembled peptide nanostructures: the design of molecular building blocks and their technological utilization. *Chem. Soc. Rev.* **2007**, *36* (8), 1263–1269.
- Mal, S. S.; Kortz, U. The Wheel-Shaped Cu_{20} Tungstophosphate $[\text{Cu}_{20}\text{Cl}(\text{OH})_{24}(\text{H}_2\text{O})_{12}(\text{P}_8\text{W}_{48}\text{O}_{184})]^{25-}$ Ion. *Angew. Chem., Int. Ed.* **2005**, *44* (24), 3777–3780.
- Mal, S. S.; Nsouli, N. H.; Dickman, M. H.; Kortz, U. Organoruthenium derivative of the cyclic $[\text{H}_7\text{P}_8\text{W}_{48}\text{O}_{184}]^{133-}$ anion: $[\{\text{K}(\text{H}_2\text{O})\}_3\{\text{Ru}(\text{p-cymene})(\text{H}_2\text{O})_4\}_4\text{P}_8\text{W}_{49}\text{O}_{186}(\text{H}_2\text{O})_2]^{27-}$. *Dalton Transac* **2007**, No. 25, 2627–2630.
- Mitchell, S. G.; Gabb, D.; Ritchie, C.; Hazel, N.; Long, D.-L.; Cronin, L. Controlling nucleation of the cyclic heteropolyanion $\{\text{P}_8\text{W}_{48}\}$: a cobalt-substituted phosphotungstate chain and network. *CrystEngComm* **2009**, *11* (1), 36–39.
- Mitchell, S. G.; Streb, C.; Miras, H. N.; Boyd, T.; Long, D.-L.; Cronin, L. Face-directed self-assembly of an electronically active Archimedean polyoxometalate architecture. *Nat. Chem.* **2010**, *2* (4), 308–312.
- Mitchell, S. G.; Boyd, T.; Miras, H. N.; Long, D.-L.; Cronin, L. Extended Polyoxometalate Framework Solids: Two Mn(II)-Linked $\{\text{P}_8\text{W}_{48}\}$ Network Arrays. *Inorg. Chem.* **2011**, *50* (1), 136–143.
- Cavka, J. H.; Jakobsen, S.; Olsbye, U.; Guillou, N.; Lamberti, C.; Bordiga, S.; Lillerud, K. P. A New Zirconium Inorganic Building Brick Forming Metal Organic Frameworks with Exceptional Stability. *J. Am. Chem. Soc.* **2008**, *130* (42), 13850–13851.
- Lammert, M.; Wharmby, M. T.; Smolders, S.; Bueken, B.; Lieb, A.; Lomachenko, K. A.; Vos, D. D.; Stock, N. Cerium-based metal organic frameworks with UiO-66 architecture: synthesis, properties

- and redox catalytic activity. *Chem. Commun.* **2015**, *51* (63), 12578–12581.
- (12) Zhang, J.-P.; Huang, X.-C.; Chen, X.-M. Supramolecular isomerism in coordination polymers. *Chem. Soc. Rev.* **2009**, *38* (8), 2385–2396.
- (13) Chen, R.; Yan, Z. H.; Kong, X. J.; Long, L. S.; Zheng, L. S. Integration of Lanthanide–Transition-Metal Clusters onto CdS Surfaces for Photocatalytic Hydrogen Evolution. *Angew. Chem., Int. Ed.* **2018**, *57* (51), 16796–16800.
- (14) Jamet, M.; Wernsdorfer, W.; Thirion, C.; Mailly, D.; Dupuis, V.; Mélinon, P.; Pérez, A. Magnetic Anisotropy of a Single Cobalt Nanocluster. *Phys. Rev. Lett.* **2001**, *86* (20), 4676–4679.
- (15) Kong, X.-J.; Ren, Y.-P.; Long, L.-S.; Zheng, Z.; Huang, R.-B.; Zheng, L.-S. A Keplerate Magnetic Cluster Featuring an Icosidodecahedron of Ni(II) Ions Encapsulating a Dodecahedron of La(III) Ions. *J. Am. Chem. Soc.* **2007**, *129* (22), 7016–7017.
- (16) Cremades, E.; Gómez-Coca, S.; Aravena, D.; Alvarez, S.; Ruiz, E. Theoretical Study of Exchange Coupling in 3d-Gd Complexes: Large Magnetocaloric Effect Systems. *J. Am. Chem. Soc.* **2012**, *134* (25), 10532–10542.
- (17) Peng, J.-B.; Zhang, Q.-C.; Kong, X.-J.; Ren, Y.-P.; Long, L.-S.; Huang, R.-B.; Zheng, L.-S.; Zheng, Z. A 48-Metal Cluster Exhibiting a Large Magnetocaloric Effect. *Angew. Chem., Int. Ed.* **2011**, *50* (45), 10649–10652.
- (18) Peng, J.-B.; Kong, X.-J.; Zhang, Q.-C.; Orendáč, M.; Prokleska, J.; Ren, Y.-P.; Long, L.-S.; Zheng, Z.; Zheng, L.-S. Beauty, Symmetry, and Magnetocaloric Effect—Four-Shell Keplerates with 104 Lanthanide Atoms. *J. Am. Chem. Soc.* **2014**, *136* (52), 17938–17941.
- (19) Yang, X.; Schipper, D.; Jones, R. A.; Lytwak, L. A.; Holliday, B. J.; Huang, S. Anion-Dependent Self-Assembly of Near-Infrared Luminescent 24- and 32-Metal Cd–Ln Complexes with Drum-like Architectures. *J. Am. Chem. Soc.* **2013**, *135* (23), 8468–8471.
- (20) Zhang, Q.; Lei, M.; Yan, H.; Wang, J.; Shi, Y. A Water-Stable 3D Luminescent Metal–Organic Framework Based on Heterometallic [Eu^{III}₆Zn^{II}] Clusters Showing Highly Sensitive, Selective, and Reversible Detection of Ronidazole. *Inorg. Chem.* **2017**, *56* (14), 7610–7614.
- (21) Christie, L. G.; Surman, A. J.; Scullion, R. A.; Xu, F.; Long, D.-L.; Cronin, L. Overcoming the Crystallization Bottleneck: A Family of Gigantic Inorganic {Pd_x}L ($x = 84, 72$) Palladium Macrocycles Discovered using Solution Techniques. *Angew. Chem., Int. Ed.* **2016**, *55* (41), 12741–12745.
- (22) Scullion, R. A.; Surman, A. J.; Xu, F.; Mathieson, J. S.; Long, D.-L.; Haso, F.; Liu, T.; Cronin, L. Exploring the Symmetry, Structure, and Self-Assembly Mechanism of a Gigantic Seven-Fold Symmetric {Pd₈₄} Wheel. *Angew. Chem., Int. Ed.* **2014**, *53* (38), 10032–10037.
- (23) Xu, F.; Miras, H. N.; Scullion, R. A.; Long, D. L.; Thiel, J.; Cronin, L. Correlating the magic numbers of inorganic nanomolecular assemblies with a molecular-ring Rosetta Stone. *Proc. Natl. Acad. Sci. U. S. A.* **2012**, *109* (29), 11609–11612.
- (24) Tasiopoulos, A. J.; Vinslava, A.; Wernsdorfer, W.; Abboud, K. A.; Christou, G. Giant Single-Molecule Magnets: A{Mn₈₄} Torus and Its Supramolecular Nanotubes. *Angew. Chem., Int. Ed.* **2004**, *43* (16), 2117–2121.
- (25) Vinslava, A.; Tasiopoulos, A. J.; Wernsdorfer, W.; Abboud, K. A.; Christou, G. Molecules at the Quantum–Classical Nanoparticle Interface: Giant Mn₇₀ Single-Molecule Magnets of ~4 nm Diameter. *Inorg. Chem.* **2016**, *55* (7), 3419–3430.
- (26) Liu, T.; Diemann, E.; Li, H.; Dress, A. W. M.; Müller, A. Self-assembly in aqueous solution of wheel-shaped Mo₁₅₄ oxide clusters into vesicles. *Nature* **2003**, *426* (6962), 59–62.
- (27) Müller, A.; Krickemeyer, E.; Meyer, J.; Bögge, H.; Peters, F.; Plass, W.; Diemann, E.; Dillinger, S.; Nonnenbruch, F.; Randerath, M.; Menke, C. [Mo₁₅₄(NO)₁₄O₄₂₀(OH)₂₈(H₂O)₇₀]^{(25±5)-}: A Water-Soluble Big Wheel with More than 700 Atoms and a Relative Molecular Mass of About 24000. *Angew. Chem., Int. Ed. Engl.* **1995**, *34* (19), 2122–2124.
- (28) Wang, R.; Liu, H.; Carducci, M. D.; Jin, T.; Zheng, C.; Zheng, Z. Lanthanide Coordination with α -Amino Acids under Near Physiological pH Conditions: Polymetallic Complexes Containing the Cubane-Like [Ln₄(μ_3 -OH)₄]⁸⁺ Cluster Core. *Inorg. Chem.* **2001**, *40* (12), 2743–2750.
- (29) Wang, R.; Selby, H. D.; Liu, H.; Carducci, M. D.; Jin, T.; Zheng, Z.; Anthis, J. W.; Staples, R. J. Halide-Templated Assembly of Polynuclear Lanthanide-Hydroxo Complexes. *Inorg. Chem.* **2002**, *41* (2), 278–286.
- (30) Kong, X.-J.; Wu, Y.; Long, L.-S.; Zheng, L.-S.; Zheng, Z. A Chiral 60-Metal Sodalite Cage Featuring 24 Vertex-Sharing [Er₄(μ_3 -OH)₄] Cubanes. *J. Am. Chem. Soc.* **2009**, *131* (20), 6918–6919.
- (31) Zheng, X.-Y.; Jiang, Y.-H.; Zhuang, G.-L.; Liu, D.-P.; Liao, H.-G.; Kong, X.-J.; Long, L.-S.; Zheng, L.-S. A Gigantic Molecular Wheel of {Gd₁₄₀} : A New Member of the Molecular Wheel Family. *J. Am. Chem. Soc.* **2017**, *139* (50), 18178–18181.
- (32) Li, S.-R.; Wang, H.-Y.; Su, H.-F.; Chen, H.-J.; Du, M.-H.; Long, L.-S.; Kong, X.-J.; Zheng, L.-S. A Giant 3d-4f Polyoxometalate Super-Tetrahedron with High Proton Conductivity. *Small Methods* **2021**, *5* (3), 2000777.
- (33) Du, M.-H.; Zheng, X.-Y.; Kong, X.-J.; Long, L.-S.; Zheng, L.-S. Synthetic Protocol for Assembling Giant Heterometallic Hydroxide Clusters from Building Blocks: Rational Design and Efficient Synthesis. *Matter* **2020**, *3* (4), 1334–1349.
- (34) Hou, Y.; Zakharov, L. N.; Nyman, M. Observing Assembly of Complex Inorganic Materials from Polyoxometalate Building Blocks. *J. Am. Chem. Soc.* **2013**, *135* (44), 16651–16657.
- (35) Zhang, G. Y.; Gadot, E.; Gan-Or, G.; Baranov, M.; Tubul, T.; Neyman, A.; Li, M.; Clotet, A.; Poblet, J. M.; Yin, P. C.; Weinstock, I. A. Self-Assembly and Ionic-Lattice-like Secondary Structure of a Flexible Linear Polymer of Highly Charged Inorganic Building Blocks. *J. Am. Chem. Soc.* **2020**, *142* (16), 7295–7300.
- (36) Chen, L.; Turo, M. J.; Gembicky, M.; Reinicke, R. A.; Schimpf, A. M. Cation-Controlled Assembly of Polyoxotungstate-Based Coordination Networks. *Angew. Chem., Int. Ed.* **2020**, *59* (38), 16609–16615.
- (37) Bai, Y.; Dou, Y. B.; Xie, L. H.; Rutledge, W.; Li, J. R.; Zhou, H. C. Zr-based metal-organic frameworks: design, synthesis, structure, and applications. *Chem. Soc. Rev.* **2016**, *45* (8), 2327–2367.
- (38) Dufaye, M.; Martin, N. P.; Duval, S.; Volkringer, C.; Ikeda-Ohno, A.; Loiseau, T. Time-controlled synthesis of the 3D coordination polymer U(1,2,3-Hbtc)₂ followed by the formation of molecular poly-oxo cluster {U₁₄} containing hemimellitate uranium(IV). *RSC Adv.* **2019**, *9* (40), 22795–22804.
- (39) Falaise, C.; Volkringer, C.; Vigier, J.-F.; Beaurain, A.; Roussel, P.; Rabu, P.; Loiseau, T. Isolation of the Large {Actinide}₃₈ Poly-oxo Cluster with Uranium. *J. Am. Chem. Soc.* **2013**, *135* (42), 15678–15681.
- (40) Martin, N. P.; Volkringer, C.; Henry, N.; Trivelli, X.; Stoclet, G.; Ikeda-Ohno, A.; Loiseau, T. Formation of a new type of uranium(IV) poly-oxo cluster {U₃₈} based on a controlled release of water via esterification reaction. *Chem. Sci.* **2018**, *9* (22), 5021–5032.
- (41) Martin, N. P.; Volkringer, C.; Roussel, P.; März, J.; Hennig, C.; Loiseau, T.; Ikeda-Ohno, A. {Np₃₈} clusters: the missing link in the largest poly-oxo cluster series of tetravalent actinides. *Chem. Commun.* **2018**, *54* (72), 10060–10063.
- (42) Sigmon, G. E.; Hixon, A. E. Extension of the Plutonium Oxide Nanocluster Family to Include {Pu₁₆} and {Pu₂₂}. *Chem. - Eur. J.* **2019**, *25* (10), 2463–2466.
- (43) Vanagas, N. A.; Higgins, R. F.; Wacker, J. N.; Asuigui, D. R. C.; Warzecha, E.; Kozimor, S. A.; Stoll, S. L.; Schelter, E. J.; Bertke, J. A.; Knope, K. E. Mononuclear to Polynuclear U^{IV} Structural Units: Effects of Reaction Conditions on U-Furoate Phase Formation. *Chem. - Eur. J.* **2020**, *26* (26), 5872–5886.
- (44) Mitchell, K. J.; Goodsell, J. L.; Russell-Webster, B.; Twahir, U. T.; Angerhofer, A.; Abboud, K. A.; Christou, G. Expansion of the Family of Molecular Nanoparticles of Cerium Dioxide and Their Catalytic Scavenging of Hydroxyl Radicals. *Inorg. Chem.* **2021**, *60* (3), 1641–1653.

- (45) Falaise, C.; Kozma, K.; Nyman, M. Thorium Oxo-Clusters as Building Blocks for Open Frameworks. *Chem. - Eur. J.* **2018**, *24* (53), 14226–14232.
- (46) Colliard, I.; Falaise, C.; Nyman, M. Bridging the Transuranics with Uranium(IV) Sulfate Aqueous Species and Solid Phases. *Inorg. Chem.* **2020**, *59* (23), 17049–17057.
- (47) Russell-Webster, B.; Lopez-Nieto, J.; Abboud, K. A.; Christou, G. Truly Monodisperse Molecular Nanoparticles of Cerium Dioxide of 2.4 nm dimensions: A $\{\text{Ce}_{100}\text{O}_{167}\}$ Cluster. *Angew. Chem., Int. Ed.* **2021**, *60* (22), 12591–12596.
- (48) Mitchell, K. J.; Abboud, K. A.; Christou, G. Atomically-precise colloidal nanoparticles of cerium dioxide. *Nature Commun.* **2017**, *8* (1), 1–7.
- (49) Wasson, M. C.; Zhang, X.; Otake, K.-I.; Rosen, A. S.; Alayoglu, S.; Krzyaniak, M. D.; Chen, Z.; Redfern, L. R.; Robison, L.; Son, F. A.; Chen, Y.; Islamoglu, T.; Notestein, J. M.; Snurr, R. Q.; Wasielewski, M. R.; Farha, O. K. Supramolecular Porous Assemblies of Atomically Precise Catalytically Active Cerium-Based Clusters. *Chem. Mater.* **2020**, *32* (19), 8522–8529.
- (50) Colliard, I.; Morrison, G.; Loye, H.-C. Z.; Nyman, M. Supramolecular Assembly of U(IV) Clusters and Superatoms with Unconventional Counterions. *J. Am. Chem. Soc.* **2020**, *142* (19), 9039–9047.
- (51) Colliard, I.; Nyman, M. Building $[\text{U}^{\text{IV}}_{70}(\text{OH})_{36}\text{O}_{64}]^{4-}$ Oxocluster Frameworks with Sulfate, Transition Metals, and U^{V} . *Chem. - Eur. J.* **2020**, *26* (54), 12481–12488.
- (52) Colliard, I.; Nyman, M. Ce(IV)₇₀ Oxosulfate Rings, Frameworks, Supramolecular Assembly, and Redox Activity. *Angew. Chem., Int. Ed.* **2021**, *60* (13), 7308–7315.
- (53) Øien-Ødegaard, S.; Bazioti, C.; Redekop, E. A.; Prytz, Ø.; Lillerud, K. P.; Olsbye, U. A Toroidal Zr 70 Oxysulfate Cluster and Its Diverse Packing Structures. *Angew. Chem., Int. Ed.* **2020**, *59* (48), 21397–21402.
- (54) Miras, H. N.; Cooper, G. J. T.; Long, D. L.; Bogge, H.; Muller, A.; Streb, C.; Cronin, L. Unveiling the Transient Template in the Self-Assembly of a Molecular Oxide Nanowheel. *Science* **2010**, *327* (5961), 72–74.
- (55) Wang, W.; Fullmer, L. B.; Bandeira, N. A. G.; Goberna-Ferrón, S.; Zakharov, L. N.; Bo, C.; Keszler, D. A.; Nyman, M. Crystallizing Elusive Chromium Polycations. *Chem.* **2016**, *1* (6), 887–901.
- (56) Wang, W.; Wentz, K. M.; Hayes, S. E.; Johnson, D. W.; Keszler, D. A. Synthesis of the Hydroxide Cluster $[\text{Al}_{13}(\mu_3\text{-OH})_6(\mu\text{-OH})_{18}(\text{H}_2\text{O})_{24}]^{15+}$ from an Aqueous Solution. *Inorg. Chem.* **2011**, *50* (11), 4683–4685.
- (57) Casey, W. H. Large Aqueous Aluminum Hydroxide Molecules. *Chem. Rev.* **2006**, *106* (1), 1–16.
- (58) Shohel, M.; Bjorklund, J. L.; Smith, J. A.; Kravchuk, D. V.; Mason, S. E.; Forbes, T. Z. Formation of Nanoscale $[\text{Ge}_4\text{O}_{16}\text{Al}_{48}(\text{OH})_{108}(\text{H}_2\text{O})_{24}]^{20+}$ from Condensation of $e\text{-GeAl}_{12}^{8+}$ Keggin Polycations**. *Angew. Chem., Int. Ed.* **2021**, *60* (16), 8755–8759.
- (59) Misra, A.; Kozma, K.; Streb, C.; Nyman, M. Beyond Charge Balance: Counter-Cations in Polyoxometalate Chemistry. *Angew. Chem., Int. Ed.* **2020**, *59* (2), 596–612.
- (60) Henry, M.; Jolivet, J. P.; Livage, J. Aqueous chemistry of metal cations: Hydrolysis, condensation and complexation. In *Chemistry, Spectroscopy and Applications of Sol-Gel Glasses*, Reisfeld, R.; Jørgensen, C. K., Eds. Springer Berlin Heidelberg: Berlin, Heidelberg, 1992; pp 153–206.
- (61) Ray, D.; Xie, J.; White, J.; Sigmon, G. E.; Gagliardi, L.; Hixon, A. E. Experimental and Quantum Mechanical Characterization of an Oxygen-Bridged Plutonium(IV) Dimer. *Chem. - Eur. J.* **2020**, *26* (36), 8115–8120.
- (62) Sidey, V. On the effective ionic radii for ammonium. *Acta Crystallogr., Sect. B: Struct. Sci., Cryst. Eng. Mater.* **2016**, *72* (4), 626–633.
- (63) Estes, S. L.; Antonio, M. R.; Soderholm, L. Tetravalent Ce in the Nitrate-Decorated Hexanuclear Cluster $[\text{Ce}_6\mu_3\text{-O})_4(\mu_3\text{-OH})_4]^{12+}$: A Structural End Point for Ceria Nanoparticles. *J. Phys. Chem. C* **2016**, *120* (10), 5810–5818.
- (64) Hennig, C.; Ikeda-Ohno, A.; Kraus, W.; Weiss, S.; Pattison, P.; Emerich, H.; Abdala, P. M.; Scheinost, A. C. Crystal Structure and Solution Species of Ce(III) and Ce(IV) Formates: From Mononuclear to Hexanuclear Complexes. *Inorg. Chem.* **2013**, *52* (20), 11734–11743.